Indonesian Journal of Science & Technology

Journal homepage: http://ejournal.upi.edu/index.php/ijost/

Modification of Kaolin with Carbon Quantum Dots as Composite for Methylene Blue Removal: Literature Review and Experiment

Nonni Soraya Sambudi[1,], Yuvan Sithambaran[2], Khee Chung Hui[2], Muhammad Wahyu Nugraha[3], Norashikin Ahmad Kamal[4], Noorfidza Yub Harun[2], Suriati Sufian[2]*

[1]Department of Chemical Engineering, Universitas Pertamina, Simprug, Jakarta Selatan 12220, Indonesia
[2]Department of Chemical Engineering, Universiti Teknologi PETRONAS, Seri Iskandar, 32610 Perak, Malaysia
[3]Department of Chemistry, Graduate School of Natural Science and Technology, Okayama University, Okayama 700-8530, Japan
[4]Department of Civil Engineering, Universiti Teknologi MARA (UiTM) Shah Alam, Selangor, 40450, Malaysia
Correspondence: E-mail: nonni.ss@universitaspertamina.ac.id

ABSTRACT

The modification of kaolin with nano-size fillers has exhibited excellent performance in the adsorption process. Carbon quantum dots (CQDs) are the new generation of nanoparticles that have attracted interest for their utilization as modifiers. In this study, a composite of metakaolin(MK)/CQDs was synthesized and tested for methylene blue (MB) removal. The heating and acid-alkali treatment of kaolin transformed it into MK. The interaction between MK and CQDs was analyzed using XPS to detect the binding of pyridic NH_2 and C-N. By loading CQDs into the kaolin matrix, the surface area was improved and the removal of MB increased. For a lower MB concentration at 5 ppm, the removal efficiency could reach 96%. The composite exhibited good regeneration through the recyclability test.

ARTICLE INFO

Article History:
Submitted/Received 29 May 2022
First revised 05 Jun 2022
Accepted 20 Aug 2022
First vailable online 22 Aug 2022
Publication date 01 Sep 2022

Keyword:
Adsorption,
Carbon quantum dots, Kaolin,
Methylene blue.

1. INTRODUCTION

Industries (such as textile, leather, paper, and pulp) commonly use synthetic dyes for coloring purposes. The textile industry contributes the highest amount of dye effluent (Katheresan *et al*., 2018). Around 700,000 tonnes of coloring dyes are manufactured each year, amounting to around 100,000 commercially accessible dyes to date (Katheresan *et al*., 2018).

These dye effluents lead to serious environmental concerns. Even at a low concentration in the water body, the dyes can disturb the growth of aquatic life due to their reflective and absorptive characteristics toward sunlight, which interferes with photosynthesis (Natarajan *et al*., 2018). Additionally, the consumption of dye-contaminated water could lead to central nervous system disorders, infections of the skin and eye, respiratory problems, and immune suppression (Natarajan *et al*., 2018).

Therefore, the removal of dye has become an area of interest for many researchers. Various methods have been employed to mitigate the issue, such as adsorption, advanced oxidation process, Fenton reaction, ozonation, photochemical process, coagulation and flocculation, ion exchange, and filtration (Katheresan *et al*., 2018). Adsorption is the most effective method as it prevents the formation of unwanted intermediate components, and operates with lesser contact time. Besides that, adsorption operates at a low cost with a simple design and mechanism (Awad *et al*., 2019; Fadillah *et al*., 2020; Natarajan *et al*., 2018).

Nanocomposites offer high porosity and surface area, which effectively allow them to capture cations. Nanocomposites also have high chemical reactivity, binding capacity, and versatility upon modification, which makes them ideal for the adsorption process (Awad *et al*., 2019; Fadillah *et al*., 2020; Mohapi *et al*. 2020). The utilization of natural materials such as clay for adsorption has gathered much interest due to their unique layered morphology, characteristics, abundance, and excellent adsorption properties (Awad *et al*., 2019; Mohapi *et al*., 2020).

Kaolin is abundantly found in nature and has shown the potential to be used as a low-cost adsorbent for toxic pollutants in aquatic environments. It has high chemical stability, cation exchange capacity, modifiable layered structure, small negative charge, and high specific surface area (Asuha *et al*., 2020; Fei *et al*., 2020; Lertcumfu *et al*., 2020; Mustapha *et al*., 2019). Its layered mineral structure consists of alumina octahedral and silica tetrahedral sheets with shared oxygen atoms. In addition, the surface of alumina octahedral layers is covered with hydroxyl groups that enable bridging between the layers through hydrogen bonds (Asuha *et al*., 2020; Fei *et al*., 2020; Lertcumfu *et al*., 2020). The enhancement of surface properties and adsorption ability of kaolin can be done through activation and calcination of materials. The calcination of kaolin has shown to induce its reactivity, with the temperature used usually ranging from 550 to 950°C, which changes the material to metakaolin (MK) (Asuha *et al*., 2020; Caballero *et al*., 2019; David *et al*., 2020).

The heating process also removes the impurities and improves the surface area of kaolin (Mustapha *et al*., 2019; Zhang *et al*., 2019a). However, calcination could affect the structural integrity of kaolin, and eliminate the hydroxyl group (Asuha *et al*., 2020; Niu *et al*., 2019). Therefore, acid and alkali treatments were performed by many researchers to increase the surface area and surface functional groups (Asuha *et al*., 2020; Boukhemkhem & Rida, 2017; Niu *et al*., 2019; Valeev *et al*., 2020).

Further improvement of kaolin performance for the removal of cationic dyes has been performed using various types of nanoparticles, such as Fe_3O_4, TiO_2,

DOI: http://dx.doi.org/10.xxxxx/ijost.vXiX
p- ISSN 2528-1410 e- ISSN 2527-8045

and $CuFe_2O_4$, as well as carbonaceous material such as carbon nanotube and graphene oxide (GO) (Alfred *et al*., 2020; Awad *et al*., 2019; Fei *et al*., 2020; He *et al*., 2018; Meigoli Boushehrian *et al*., 2020; Wongso *et al*., 2019).

CQDs is an attractive nanomaterial with good chemical and optical stability, high specific surface area, and excellent adsorption capability (Chung Hui *et al*., 2021; Liu *et al*., 2017b; Wongso *et al*., 2020; Yahaya Pudza *et al*., 2020; Zainal Abidin *et al*., 2020). The adsorption performance of CQDs has been tested for the removal of heavy metals such as cadmium and lead also for the removal of cationic dyes in the form of composites (de Oliveira *et al*., 2020; Yahaya Pudza *et al*., 2020; Yang *et al*., 2019; Yin *et al*., 2020; Zainal Abidin *et al*., 2020).

The adsorption of pollutants can be greatly enhanced by incorporating CQDs into the matrix of kaolin, which could facilitate the addition of abundant surface functional groups. As a result, the adsorption performance is enhanced through van der Waals forces, hydrogen bonds, or even electrostatic attraction with pollutants (Yahaya Pudza *et al*., 2020; Yin *et al*., 2020). To the best of our knowledge, the combination of kaolin with CQDs for the removal of pollutants remains limitedly explored. In this study, CQDs were loaded into the kaolin matrix, and the composite was characterized by its crystallinity, functional groups, and surface area.

The composite showed an increase in surface area, which led to the enhancement of methylene blue (MB) dye removal for MB concentrations ranging from 5 to 20 ppm. The sample was then re-used to study its potential for recyclability. The fitting for the kinetic models was performed based on the collected adsorption data.

2. LITERATURE REVIEW

2.1. Kaolin

Many different separation techniques, such as physical, chemical, and adsorption processes, have been used to separate dyes from wastewater. From the techniques stated above, physical and chemical processes are found to be too costly and not environmentally friendly. Therefore, adsorption is an excellent technique to remove dissolved organic pollutants such as dyes from wastewater (Kandisa & K.V, 2016). Adsorption is a process that mainly utilizes surface forces (Ragadhita & Nandiyanto, 2021).

Adsorption happens when the adsorbate is being adsorbed by the adsorbent, which has a great porous surface structure and liquid-solid intermolecular forces of attraction (Ragadhita & Nandiyanto, 2021). A low-cost adsorbent is defined as one that is abundant in nature or is a by-product or waste from industries, and requires little to no processing (Dewi *et al*., 2021; Fiandini, 2020; Nandiyanto *et al*., 2022a).

Clay minerals act as good adsorbents because of their characteristics of having large surface areas relative to their small particle size and high cation exchange capacity (Awad *et al*., 2019). Hence, their surface reactions have significant biochemical and environmental effects on the soil and water. Such minerals can be used extensively because they are abundant and available at a lower cost. These advantages support the use of minerals in the decontamination and remediation treatment process.

Table 1 represents the removal of various chemical pollutants and dyes in wastewater or solution by utilizing different types of adsorbents.

DOI: http://dx.doi.org/10.xxxxx/ijost.vXiX
p- ISSN 2528-1410 e- ISSN 2527-8045

Table 1. Performance of adsorbents on the removal of pollutants in an aqueous system.

No	Type of Adsorbent	Parameter	Condition	Pollutant Model	Reference
1	Tamazert Kaolin	pH Concentration Dosage Temperature Adsorption Capacity	7.2 100-400 mg/L 10 g/l 30°C 7.2 mg/g	Methylene blue	(Boukhemkhem & Rida, 2017)
2	Activated Carbon from Rice Husk Ash	pH Concentration Dosage Temperature Adsorption Capacity	4-8 50 mg/L - 26-34°C 3.9370 mg/g	Phenol	(Anshar *et al.*, 2016)
3	Bentonites	pH Concentration Dosage Temperature Adsorption Capacity	11-12 500-800 mg/L - 25°C 357.1-500 mg/g	Methylene blue	(Çiftçi, 2022)
4	Saudi Red Clay	pH Concentration Dosage Temperature Adsorption Capacity	6.4 100 mg/L 0.3 g/L 25°C 50.25 mg/g	Methylene blue	(Khan, 2020)
5	Zeolites from Coal Fly Ash	pH Concentration Dosage Temperature Adsorption Capacity	- 100 mg/L - - 18.025 mg/g	Ammonium	(Prihastuti & Kurniawan, 2022)
6	Activated Carbon from Coconut Shell	pH Concentration Dosage Temperature Adsorption Capacity	8 250 mg/L 0.1 g/L - 15.775 mg/g	Methylene blue	(Khuluk *et al.*, 2019)
7	Natural Zeolite (size of 3000 µm)	pH Concentration Dosage Temperature Adsorption Capacity	- 10-90 mg/L - - 181.8-421.49 mg/g	Curcumin	(Nandiyanto *et al*., 2022b)
8	ZIF-8	pH Concentration Dosage Temperature Adsorption Capacity	- 20-80 mg/L - - 11.668 mg/g	Curcumin	(Ragadhita & Nandiyanto, 2022)
9	Silica from Rice Husk	pH Concentration Dosage Temperature Adsorption Capacity	- 50 mg/L 0.1 g/L - 82.64 mg/g	Curcumin	(Ragadhita *et al*., 2019)
10	Kaolin-Bentonite	pH Concentration Dosage Temperature Adsorption Capacity	9.1 50-400 mg/L - 25°C 12.68 mg/g	Rhodamine B	(He *et al.*, 2022)

DOI: http://dx.doi.org/10.xxxxx/ijost.vXiX
p- ISSN 2528-1410 e- ISSN 2527-8045

Table 1 (Continue). Performance of adsorbents on the removal of pollutants in an aqueous system.

No	Type of Adsorbent	Parameter	Condition	Pollutant Model	Reference
11	Moroccan Clay	pH Concentration Dosage Temperature Adsorption Capacity	11 100-900 mg/L 0.5 g/L 60°C 456.62 mg/g	Methylene blue	(Loutfi *et al.*, 2022)
12	Kaolin (from Nigeria)	pH Concentration Dosage Temperature Adsorption Capacity	5.84 - 0.2 g/L - 459.896 mg/g	Sulfate in tannery wastewater	(Mustapha *et al.*, 2019)
13	Kaolin/ZnO	pH Concentration Dosage Temperature Adsorption Capacity	5.84 - 0.2 g/L 29°C 117.25 mg/g	Cr(VI) from tannery wastewater	(dMustapha *et al.*, 2020)

Kaolin is a type of clay mineral with a 1:1 layer ratio of tetrahedral silica and octahedral aluminum sheets (Zhang *et al.*, 2021). Clay minerals can be found in soil and deposits, and are made up of phyllosilicates with sizes smaller than 2 µm. They are composed of layered units of one or two tetrahedral silica sheets attached to an octahedral aluminum sheet (Guggenheim & Martin, 1995; Zhang *et al.*, 2021).

The complex structure of clay can be modified, pre-treated, and combined with other materials to produce an adsorbent with a high surface area. In addition, most types of clays have negatively charged surfaces that can attract cationic pollutants and facilitate the ion-exchange process (Zhang *et al.*, 2021). The negatively charged surface is the result of isomorphic substitution in the tetrahedral and/or octahedral sheets (Zhang *et al.*, 2019).

Kaolin and zeolite are two good examples of low-cost natural mineral adsorbents, as shown in **Table 1**. The uptake of pollutants onto the surface of kaolin is regulated by ion exchange if the uptake does not exceed the cation-exchange capacity, and by hydrophobic bonding, if the uptake exceeds the cation-exchange capacity (Sen Gupta & Bhattacharyya, 2012). Besides that, the type of pollutants determines the efficiency of surface adsorption, as the interactions can occur through weak van der Waals bonding, hydrophobic effects, hydrogen bonding, or even ligand complex formation (Sen Gupta & Bhattacharyya, 2012).

2.2. Carbon Quantum Dots

Functional groups with an abundance of oxygen atoms (e.g., -OH, -COOH, C=O) are present on the surface of CQDs (Rani *et al.*, 2020). With the presence of these oxygen-containing functional groups and low toxicity, CQDs are the best alternative material for the adsorption of contaminants, especially for organic pollutants and heavy metals (Rani *et al.*, 2020).

The adsorption process on the surface of CQDs can occur through physical and chemical interactions through the availability of functional groups. Functional groups (such as amines and carboxyls) can facilitate the binding of metal ions through π-π stacking and electrostatic attraction (Rani *et al.*, 2020). The modification of CQDs with nitrogen- and oxygen-containing

DOI: http://dx.doi.org/10.xxxxx/ijost.vXiX
p- ISSN 2528-1410 e- ISSN 2527-8045

functional groups create active sites for the adsorption of metal ions (Chung Hui *et al*., 2021; Zainal Abidin *et al*., 2020).

The experimental data for the removal of methyl orange with CQDs/$ZnFe_2O_4$ suggests the inclusion of van der Waals forces besides electrostatic attraction in the adsorption process (Shi *et al*., 2018). A previous study by Liu *et al*. investigated the removal of tetracycline using NiFe/CQDs, and the results showed that the high adsorption of the antibiotic can be ascribed to surface complexation, electrostatic interaction, and cation-exchange between tetracycline and the CQDs composite (Liu *et al*., 2017a). The synergistic effects of surface complexation, π-π bonding, covalent bonding, electrostatic interaction, and cation exchange determine the adsorption performance of CQDs (Long *et al*., 2021).

3. METHOD

3.1. Materials

Kaolin was obtained from Kaolin (M) Sdn. Bhd. (Malaysia). CQDs were sourced from rice husks that were collected from Jabatan Pertanian Negeri Perak, Malaysia. MB, the model dye used in this study, was obtained from Bendosen (Malaysia). Sodium hydroxide (NaOH) was purchased from Sigma Aldrich (USA). Hydrochloric acid (HCl) 37% was purchased from Merck (USA). Deionized (DI) water was used for the preparation of solutions, and all chemicals were used as received.

3.2. Synthesis of CQDs

CQDs were synthesized from rice husks with modifications from the methodology by Chung *et al*. (2020). One gram of rice husks was collected and washed thoroughly with DI water to remove impurities. The husks were then dried and blended until powdered consistency was obtained. The powdered sample was then oxidized using 0.1 M HCl and centrifuged at 4000 rpm for 15 minutes (min).

The powdered sample was then washed three times using DI water through centrifugation at 4000 rpm for 15 min. The obtained samples were oven-dried overnight at 80°C. A sample of 100 mg dried rice husk powder was then placed inside a Teflon-lined autoclave with 20 mL DI water. The solution was heated at 190°C for 12 h. After heating, the solution was cooled down to room temperature, followed by vacuum filtration and centrifugation to obtain the CQDs supernatant. The supernatant was dialyzed in DI water overnight to obtain purified CQDs.

3.3. Modification of Kaolin and Kaolin/CQDs

The modification of kaolin was adapted from the method by Boukhemkhem & Rida, (2017), where pristine kaolin was heated at 800°C for 5 hours (h) to obtain MK and remove impurities. 30 g of MK was then treated with 60 mL of 2.5 M HCl solution at 80°C for 7 h. The sample was then washed with distilled water and dried in an oven at 110°C for 3 h. This step was followed by alkali treatment with 60 mL of 0.5 M NaOH solution under similar conditions as acid treatment. Later, the samples were washed and dried. To obtain kaolin/CQDs samples, 10, 20, and 40 mL of CQDs were mixed with and processed with both acid and alkali treatment to produce MK/CQD(10), MK/CQD(20), and MK/CQD(40).

3.4 Characterization of Synthesized Materials

The morphology of CQDs was characterized using high-resolution transmission electron microscopy (HRTEM) (Tecnai G2 20 S-Twin), and Fourier Transforms Infrared Analysis (FTIR, Perkin Elmer) from 500 to 4000 cm^{-1} (Nandiyanto *et al*., 2019). The photoluminescence (PL) of CQDs was verified using a PL spectrophotometer (Edinburgh Instrument FLS920) with 420 nm as excitation wavelength.

DOI: http://dx.doi.org/10.xxxxx/ijost.vXiX
p- ISSN 2528-1410 e- ISSN 2527-8045

The crystallinity and functional groups of pristine kaolin, MK and MK/CQD, were analyzed using X-ray powder diffraction (XRD, Bruker D8) and Fourier transform infrared analysis (FTIR, Perkin Elmer) from 500 to 4000 cm^{-1} (Fatimah *et al.*, 2021; Obinna, 2022; Sukamto & Rahmat, 2022), respectively. The morphologies of pristine kaolin, MK, and MK/CQD were characterized using field emission scanning electron microscopy (FESEM, Zeiss Supra 55 VP) (Yolanda & Nandiyanto, 2021), and both the surface area and pore diameter of the samples were identified using Micrometrics ASAP 2020 Plus.

The point of zero charges (pHpzc) of the samples was determined using the pH floating method (Li *et al.*, 2018). A series of vials containing 20 mL of DI water was prepared, with initial pH values of 2, 4, 7, 10, and 12. 0.1 M HCl and 0.1 M NaOH were used to adjust the pH. Then, each vial was filled with 50 mg of MK and MK/CQD samples and kept for 24 h to achieve equilibrium at 25°C. The final pH values were calculated and plotted against the initial pH. Herein, the pHpzc value was determined from the graph as the point of intersection where the initial pH vs final pH curve meets the $y = x$ line.

The elemental compositions on the samples were analyzed using a K-Alpha X-ray Photoelectron Spectrophotometer (XPS) (Thermo Fisher Scientific, USA) equipped with an Al K(alpha) radiation source with a spot size of 400 m. The XPS was run with constant analyzer energy (CAE) at a pass energy of 200 eV and a step size of 1.0 eV. Deconvolution of peaks was done using the Gaussian functions in the OriginPro 2018 software.

3.5. Adsorption of MB

The concentration of MB at 10 ppm was prepared with 100 mL distilled water and mixed with the adsorbent. This solution was continuously shaken at 200 rpm. Samples were taken at the time intervals of 15, 30 min, 1, 2, 4, 6, and 8 h, and characterized using a UV Vis spectrophotometer (λ = 665 nm, Shimadzu UV-1800). The % removal of MB was calculated with Eq. (1) as follows:

$$\% \text{ removal} = \frac{C_0 - C_t}{C_0} \times 100\% \quad (1)$$

where C_0 is the initial concentration and C_t is the concentration at a specific time interval. For the effect of adsorbent amount, the amount of MK was varied at 1, 2, 3, 4, and 5 g at the MB concentration of 10 ppm.

The amount of adsorbent at 5 g was then used for MK/CQD samples. Initial MB concentrations at 5, 10, 15, and 20 ppm were prepared, and the solution sample was measured with UV Vis analysis after 8 h of adsorption. The amount of adsorption at a time, t, was calculated using Eq. (2), where V is the volume of the solution and W is the amount of adsorbent.

$$q_t = \frac{(C_0 - C_t)V}{W} \quad (2)$$

The recyclability test was performed with MK/CQD(40) using 10 ppm of MB for 4 consecutive cycles. Around 5 g of MK/CQD(40) was dispersed in 100 mL of 10 ppm of MB. The solution was stirred for 8 h, then centrifuged to collect the adsorbent. The adsorbent was then washed thoroughly with DI water before reuse. The UV Vis analysis was performed after 8 h of adsorption.

4. RESULTS AND DISCUSSION

4.1. Morphology, Functional Groups of CQD, and Surface Area

The synthesized CQDs showed spherical structures (**Figures 1a** and **1b**) with an estimated average diameter of 0.21 nm. Moreover, the synthesized CQDs were found to be fluorescent (**Figure 1c**) with an emission wavelength of approximately 440 nm. The intercalation and exfoliation of rice husks have been reported to generate CQDs through dispersion in acid and washing with

DOI: http://dx.doi.org/10.xxxxx/ijost.vXiX
p- ISSN 2528-1410 e- ISSN 2527-8045

water, respectively (Hens *et al.*,2012; Wongso *et al.*, 2019). Besides that, carbonization occurred during the hydrothermal process to produce small-sized CQDs (Wongso *et al.*, 2020). The FTIR spectrum of CQDs in **Figure 1d** shows the presence of C-H bending at 620 cm^{-1} (Raj & Chirayil, 2017; Chung Hui *et al.*, 2021), C=O bonding (carbonyl) at 1639 cm^{-1} (Raj & Chirayil, 2017;Chung Hui *et al.*, 2021; Wongso *et al.*, 2020), and O-H stretching due to carboxylic and absorbed water at 3300 cm^{-1} (Raj & Chirayil, 2017;Chung Hui *et al.*, 2021; Wongso *et al.*, 2020).

Pristine kaolin exhibited a layered structure, and stacks of kaolin sheets were observed to adhere to each other with thicknesses ranging from 20 to 60 nm (**Figure 2a**). Small fragments were rarely observed as well. However, the morphology of the material experienced changed with modification, such that the structural layers were disintegrated into fragments which can be seen along with stacks of kaolin sheets (**Figures 2b, d, f, h**). High-temperature treatment likely disrupted the morphology and caused defects to the material as have been reported in earlier studies, which could have reduced the structure size (Chai *et al.*, 2020; Vakalova *et al.*, 2019), whereas the acid-alkali treatment might have increased the spaces between particles (Boukhemkhem & Rida, 2017; Ferrazzo *et al.*, 2020).

The slit-shape pores were visible on the surface of modified kaolin (MK and MK/CQD), which contributed to the porosity of kaolin and its adsorption performance (**Figures 2c, e, g, i**).

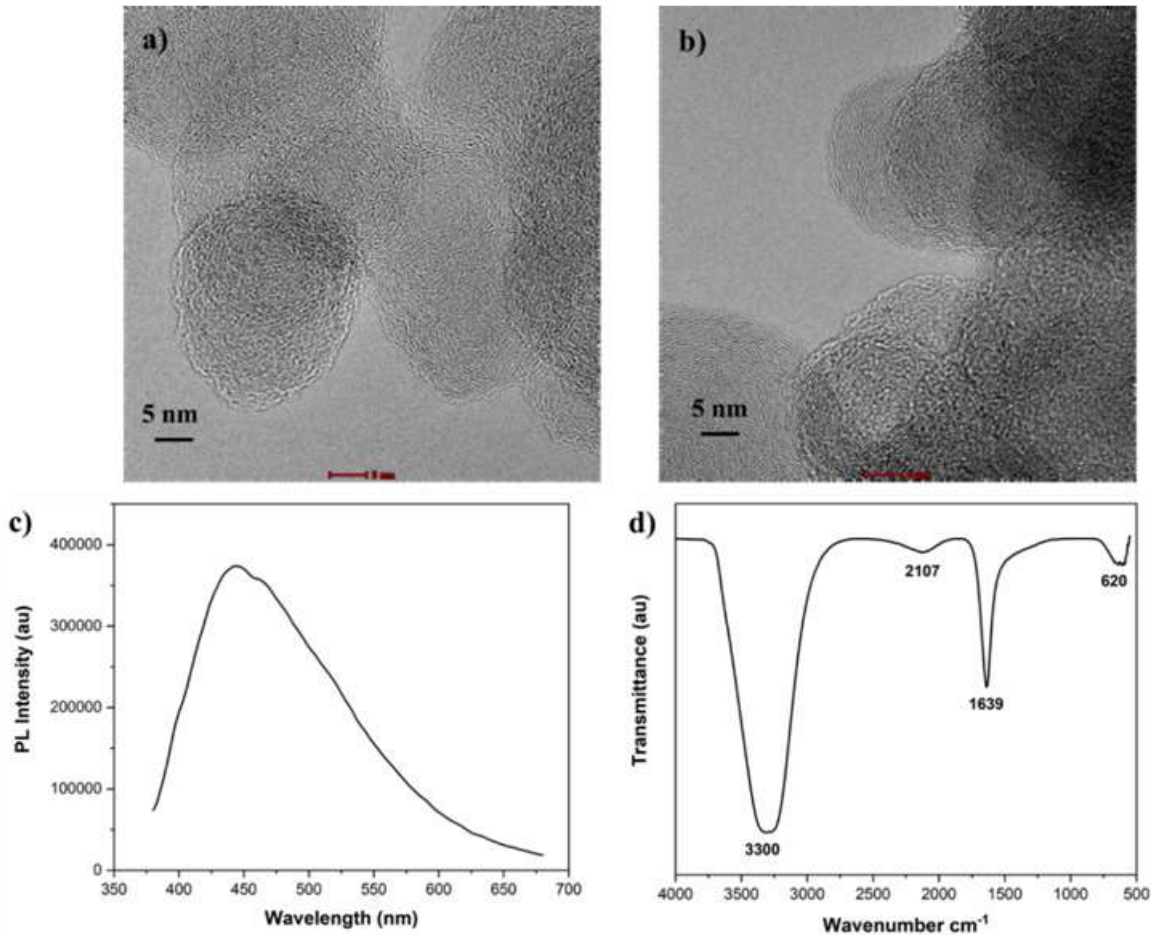

Figure 1. Morphologies (a,b), PL spectrum (b), and FTIR spectrum (d) of CQDs.

DOI: http://dx.doi.org/10.xxxxx/ijost.vXiX
p- ISSN 2528-1410 e- ISSN 2527-8045

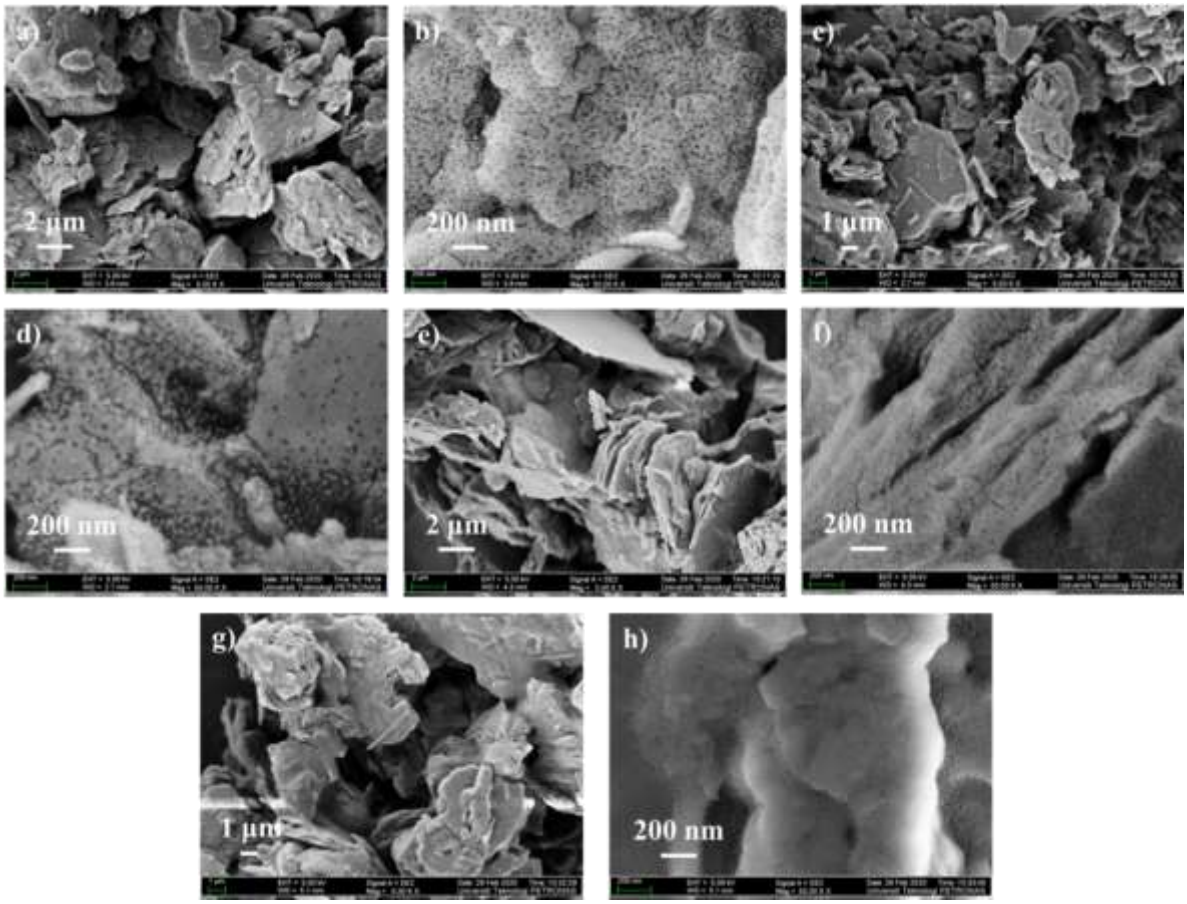

Figure 2. FESEM images of a) pristine kaolin, b) MK, c) and d) MK/CQD(10), e) and f) MK/CQD(20), g) and h) MK/CQD(40).

The surface area of pristine kaolin, MK ad MK/CQD were presented by isotherm graphs (**Figure 3**). The isotherm of pristine kaolin (**Figure 3a**) followed a type III isotherm for non-porous or macroporous material, due to compaction and aggregation of the mineral sheets (Kuila & Prasad, 2013; Thommes *et al*., 2015). On the other hand, MK and MK/CQD exhibited type IV isotherm (**Figures 3b-e**), which is typical for mesoporous materials with a pore size ranging from 3.7 to 6.22 nm. Hence, the modification successfully transformed kaolin into a porous structure.

The hysteresis loop could be observed, due to capillary condensation (Chai *et al*., 2020; Thommes *et al*., 2015). The modification of kaolin through high temperature and acid-alkali treatment improved the surface area of the material from 11.31 to 16.23 m^2/g due to the formation of mesopores (Chargui *et al*., 2018; Shu *et al*., 2014). A previous study showed similar results whereby the acid treatment of kaolin improved its surface area from 10.44 to 19.27 m^2/g (Chai *et al*., 2020).

Further improvement of the surface area could be achieved using CQDs as modifiers at 21.5, 37.23, and 46.29 m^2/g for MK/CQD(10), MK/CQD(20), and MK/CQD(40), respectively, which was 4 times the surface area of pristine kaolin. This could be due to the uniform dispersion of CQDs in kaolin to provide more adsorption sites.

DOI: http://dx.doi.org/10.xxxxx/ijost.vXiX
p- ISSN 2528-1410 e- ISSN 2527-8045

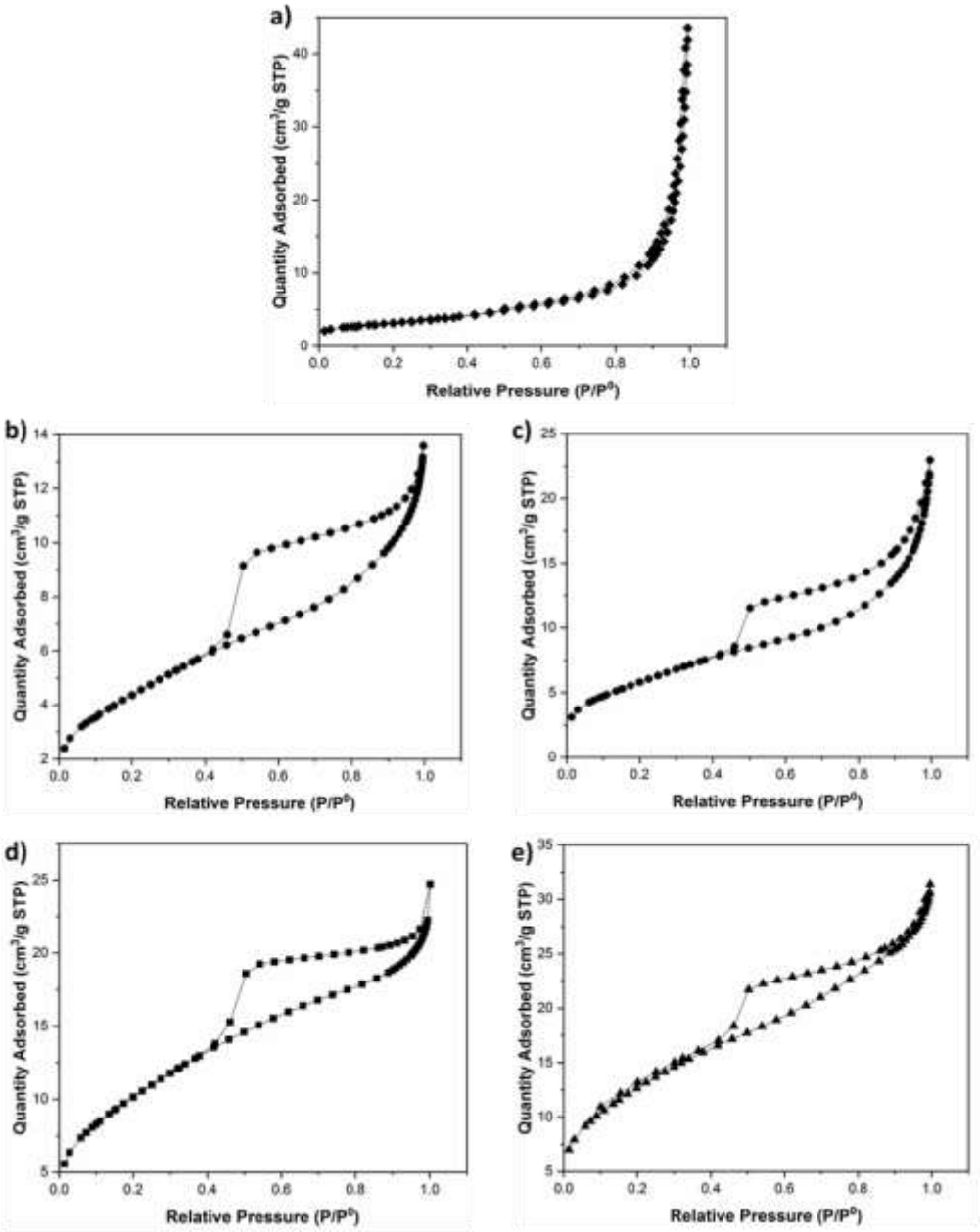

Figure 3. N_2 adsorption-desorption isotherms of a) pristine kaolin, b) MK, c) MK/CQD(10), d) MK/CQD(20), and e) MK/CQD(40).

4.2. Crystallinity and Functional Groups

The XRD spectra in **Figure 4** exhibited peaks belonging to kaolinite and quartz that build the material. Pristine kaolin showed a main peak at 24.8° (**Figure 4a**). Meanwhile, the other peaks at 19.8, 34.9, and 38.4° represent kaolinite. The material transformed to MK when the modification was performed, as shown in **Figure 4b**. The main peak of quartz could be found at 26.7°, and other peaks at 20.8, 36.7, 39.5, 45.6, and 50°.

The modified kaolin (MK and MK/CQD) contains SiO_2 at around 56, 63, 67, and 62% for MK, MK/CQD(10), MK/CQD(20), and MK/CQD(40), respectively, while the remaining comprises Al_2O_3, Fe_2O_3, TiO_2, CaO, MgO, K_2O, and Na_2O. Previous studies have shown that increased SiO_2 contents are expected when kaolin transforms into MK through heat treatment. The SiO_2 contents can vary from 50 to 60%, sometimes reaching 74.3% (Fadzil *et al.*, 2017; Pillay *et al.*, 2020; Rashad, 2013; Sullivan *et al.*, 2018).

DOI: http://dx.doi.org/10.xxxxx/ijost.vXiX
p- ISSN 2528-1410 e- ISSN 2527-8045

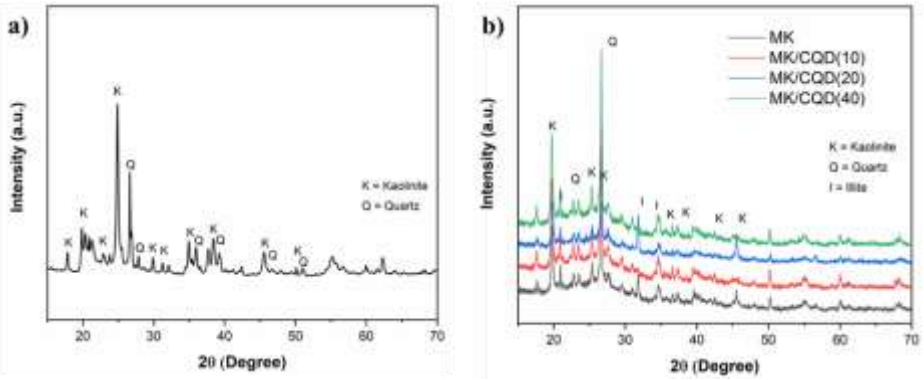

Figure 4. XRD spectra of a) pristine kaolin, b) MK, and MK/CQD.

The remainder consists of kaolinite and a small amount of muscovite. The results are in agreement with previous studies using high-temperature treatment at 700, 750, and 800°C to transform kaolin to MK, which could be due to a dihydroxylation reaction (Boukhemkhem & Rida, 2017; I. Khan *et al*., 2017; Lertcumfu *et al*., 2020). Due to the loss of the hydroxyl group, aluminum coordination changed from six-fold to a mixture of six-, five- and four-fold, which produced MK, the more reactive form of kaolin (Gasparini *et al*., 2013).

Functional groups of pristine kaolin and modified kaolin (MK and MK/CQD) are shown in **Figure 5**. For pristine kaolin, Si-O-Al stretching was assigned to the peaks at 695.5, 757, and 790.5 cm^{-1}. These peaks changed to a broad band at 790.5 cm^{-1} which was consistent with the distortion of octahedral and tetrahedral layers due to heating (Boukhemkhem & Rida, 2017; Wongso *et al*., 2019).

The peaks at 912.56 and 1034.66 cm^{-1} for pristine kaolin were attributed to Si-O-T (T: Si or Al) with asymmetric stretching vibration (Lertcumfu *et al*., 2020). These peaks also changed to a broad band at 987.57 cm^{-1} which could be due to the disappearance of Al-OH units (Boukhemkhem & Rida, 2017). These changes were consistent with the disorderly characteristic of MK (Boukhemkhem & Rida, 2017). In addition, the adsorbed water resulted in the peaks at 3614.6, 3703.1, 3370.4, 1639.5, and 1632.35 cm^{-1}, which were most likely attributed to H-O-H stretching and bending vibrations (Wongso *et al*., 2019). XPS is one of the fundamental analyses to study the chemical state of elements. **Figure 6** and **Table 2** show the full-scan XPS spectra of MK/CQD composites and the atomic percentage of each element, respectively. The prominent peaks of O1s, Al2p, Si2p, C1s, and N1s were observed throughout the composites.

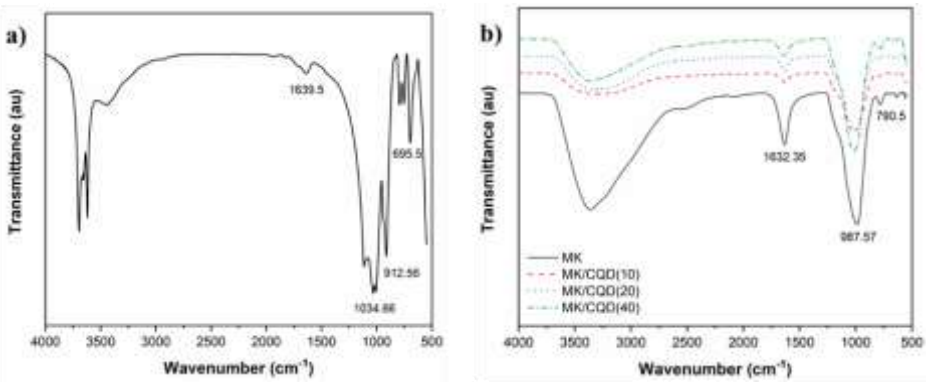

Figure 5. FTIR spectra of a) pristine kaolin, b) MK and MK/CQD.

DOI: http://dx.doi.org/10.xxxxx/ijost.vXiX
p- ISSN 2528-1410 e- ISSN 2527-8045

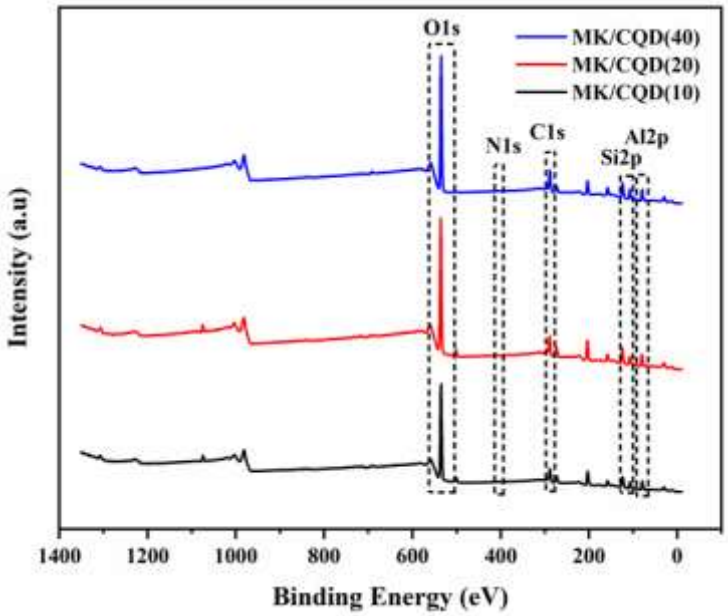

Figure 6. Full-scan XPS spectra of MK/CQD.

Table 2. The atomic percentage of MK/CQD.

Sample	Atomic percentage (at %)				
	Al	Si	O	C	N
MK/CQD(10)	18.72	10.7	51.84	18.08	0.48
MK/CQD(20)	20.63	8.93	52.1	18.27	0.26
MK/CQD(40)	17.77	10.11	51.74	20.09	0.28

The high-resolution spectra of Al2p from **Figure 7a** exhibited $Al2p_{1/2}$ and $Al2p_{3/2}$ for each MK/CQD composite. MK/CQD(10) showed binding energies of 76.08 and 77.28 eV, which corresponded to $Al2p_{1/2}$, and binding energy of 79.08 eV which corresponded to $Al2p_{3/2}$ (Lan *et al.*, 2019; Liu *et al.*, 2020; Mudgal *et al.*, 2021; Ye *et al.*, 2017). The MK/CQD(20) exhibited higher binding energies of $Al2p_{1/2}$ and $Al2p_{3/2}$ at 76.88, 77.18, 78.58, and 80.08 eV. The MK/CQD(20) also showed binding energy of 68.08 eV, which corresponded to Al metal (Liu *et al.*, 2013).

Moreover, MK/CQD(40) exhibited higher binding energies of $Al2p_{1/2}$ and $Al2p_{3/2}$ at 76.68 and 79.18 eV, respectively, as compared to MK/CQD(10). Although the difference in binding energy was small, the shift to higher binding energy was present. This chemical shift might be induced by the interaction of the deposited CQDs (Liu *et al.*, 2013). The high-resolution of Si2p from **Figure 7b** revealed that each MK/CQD composite exhibited $Si2p_{3/2}$ and $Si2p_{1/2}$ (Liu *et al.*, 2020). Higher CQDs concentration towards MK resulted in a slightly higher shift of binding energy of Si2p spectra.

Moreover, the high-resolution spectra of O1s in **Figure 7c** revealed that MK/CQD composites were rich in oxygen, shown through the binding energies of O-Al/ O-H and Si-O-T (sialate bonds)/ C-O (Lan *et al.*, 2019; Liu *et al.*, 2020; Mudgal *et al.*, 2021).

The interaction of MK and CQDs could be seen from the C1s high-resolution spectra in **Figure 7d**, where the composites exhibited C-O/C-N, C=O, and a carboxyl group (COOH) (Li *et al.*, 2017; Nugraha *et al.*, 2021; Ratlam *et al.*, 2020). Additionally, the N element was also shown through the N1s high-resolution spectra in **Figure 7e**. The MK/CQD composites showed the binding energies of pyridic NH_2 and C-N (Li *et al.*, 2017; Nugraha *et al.*, 2021; Ratlam *et al.*, 2020).

DOI: http://dx.doi.org/10.xxxxx/ijost.vXiX
p- ISSN 2528-1410 e- ISSN 2527-8045

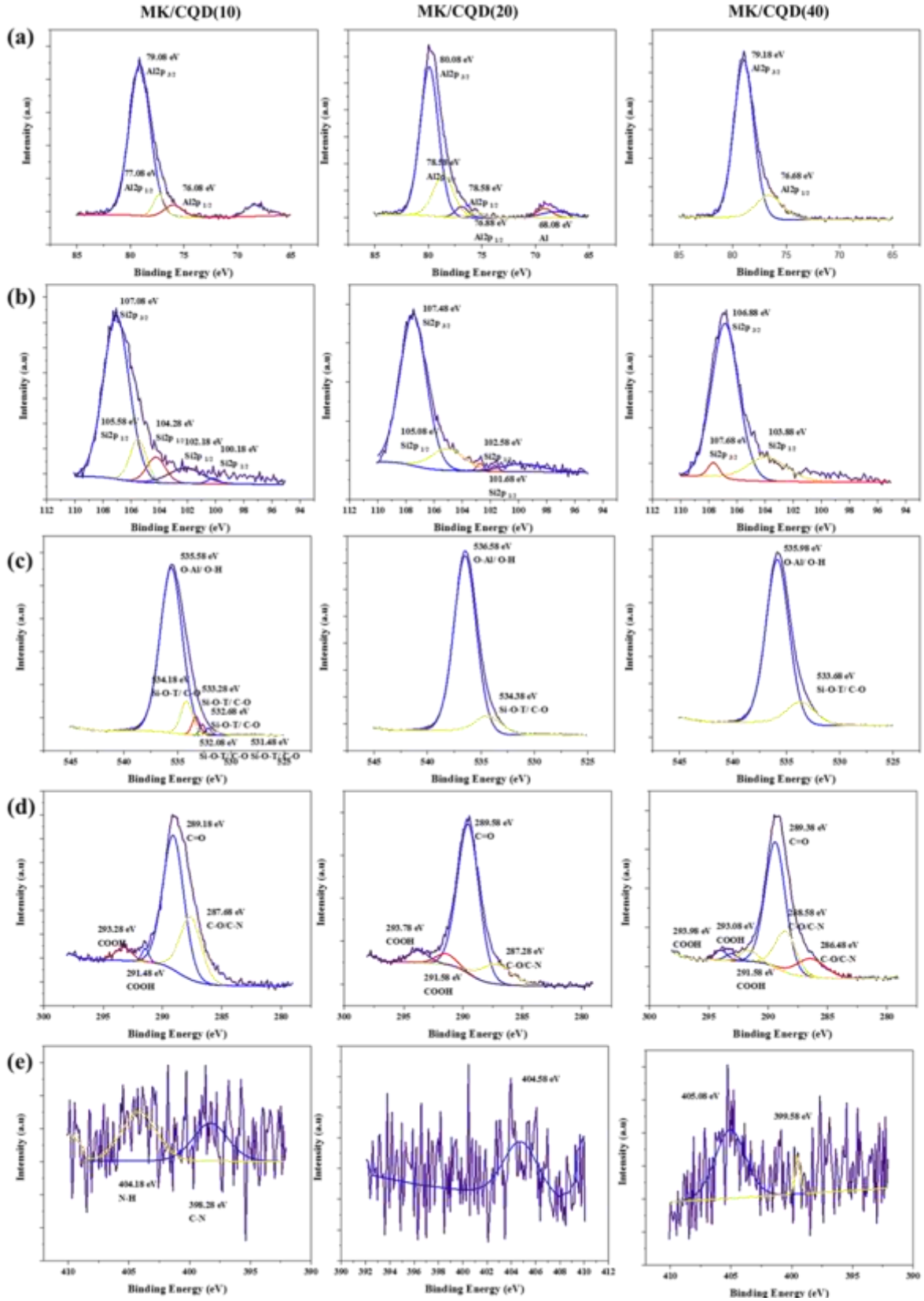

Figure 7. High-resolution XPS spectra of MK/CQD (a) Al2p, (b) Si2p, (c) O1s, (d) C1s, (e) N1s.

DOI: http://dx.doi.org/10.xxxxx/ijost.vXiX
p- ISSN 2528-1410 e- ISSN 2527-8045

4.3. Adsorption of MB

4.3.1. Effect of adsorbent amount

The adsorption test was performed on MK samples to identify the optimum amount of adsorbent required to reach maximum adsorption. One gram of adsorbent could remove approximately 35% of MB. The removal was increased further to 59.31, 59.35, and 60% with the use of 3, 4, and 5 g of adsorbent, respectively.

This was due to the presence of more active sites (**Figure 8**). Further MB removal experiments were conducted with 5 g of adsorbent to maximize the adsorption process. The removal of MB was further improved using MK/CQD as the adsorbent, with MB removal at 61.86, 71.57, and 77.04% using MK/CQD(10), MK/CQD(20), and MK/CQD(40), respectively (**Figure 9a**).

Hence, the overall efficiency of MB removal increased by 2.2-fold. The enhanced performance of MB removal could be observed for MK/CQD when the amount of CQDs loaded was increased from 10 to 40 mL. The improvement in the surface area of kaolin through heating, acid-alkali treatment, and CQDs loading resulted in a porous structure with more active sites for MB adsorption.

The surface area was successfully increased by 4 times from 11.31 to 46.29 m^2/g, which improved the efficiency of MB removal. The adsorption with MK/CQD(20) and MK/CQD(40) was reported to be more than 50% after only 30 min, which could be attributed to the abundant adsorption sites.

The adsorption was over 60% of MB after 2 h, where equilibrium was reached. The utilization of CQDs as the sole adsorbent is shown in **Figure 9b**, where approximately 40% of MB was adsorbed after 8 h. The adsorption of cations onto the surface of CQDs could happen through the electrostatic interactions of hydroxyl ions that were available on CQDs (Chung Hui *et al*., 2021; Zainal Abidin *et al*., 2020).

Similar performance was observed when graphene oxides and graphene quantum dots were used. After 8 h, approximately 40 and 20% of reactive red 2 dye were removed, respectively. This could be due to π-π interaction, hydrogen bonding, and electrostatic interaction in the samples (de la Luz-Asunción *et al*., 2020). To study the relationship between the adsorption time and adsorption capacity of MK and MK/CQD, adsorption kinetic models were constructed (**Figure 10**), and the calculated parameters are shown in **Table 3**.

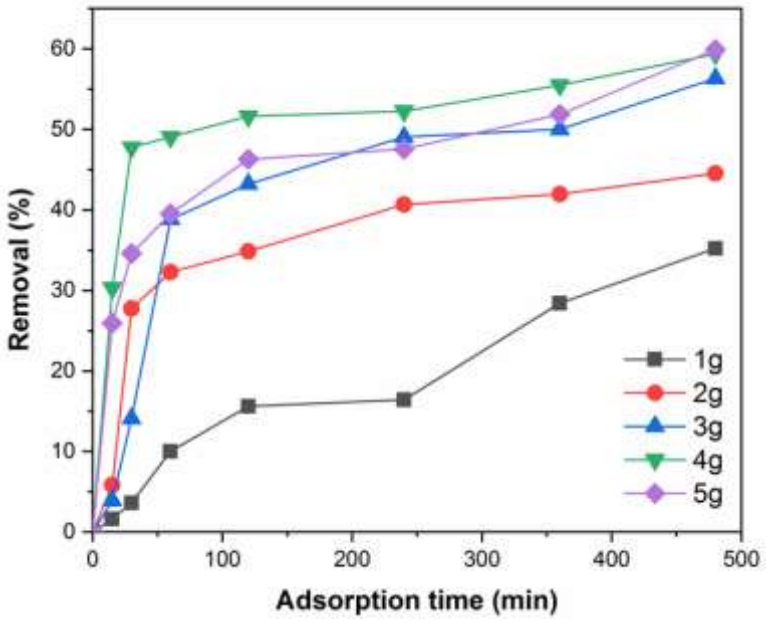

Figure 8. Effect of MK amount on removal profile of 10-ppm MB.

DOI: http://dx.doi.org/10.xxxxx/ijost.vXiX
p- ISSN 2528-1410 e- ISSN 2527-8045

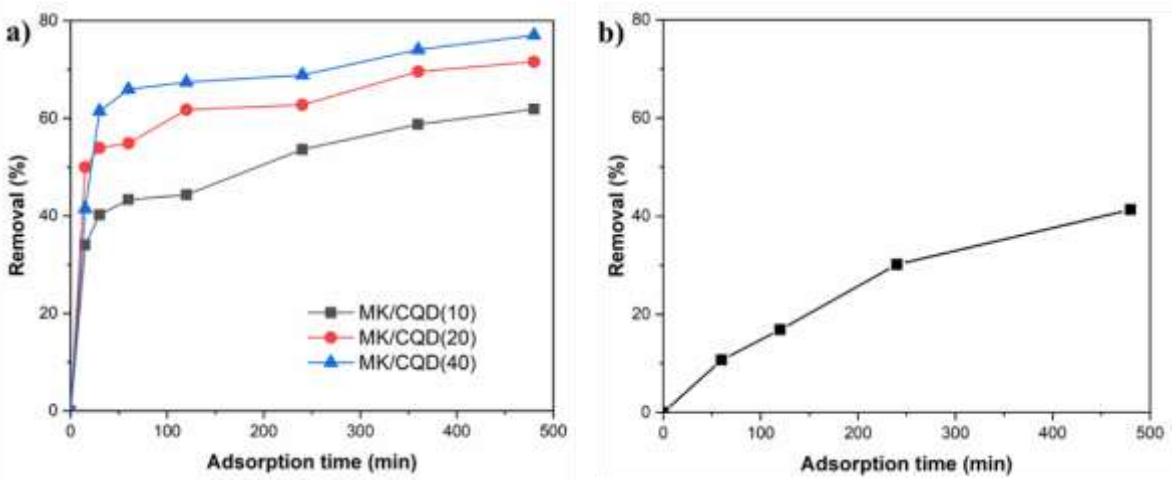

Figure 9. Removal profile of 10-ppm MB using MK/CQD (a) and CQDs (b).

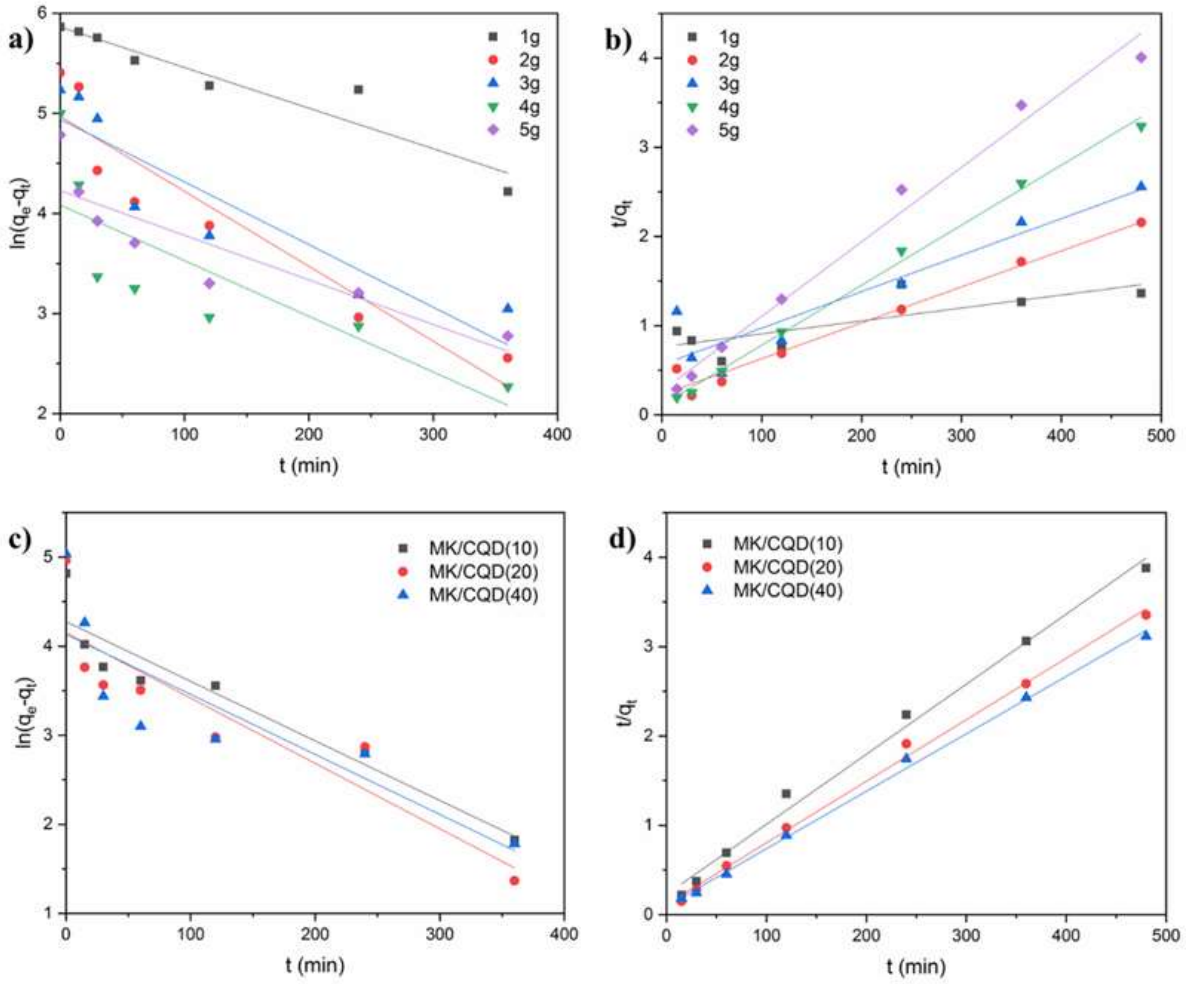

Figure 10. Pseudo-first-order kinetic models of MK (a) and MK/CQD (c). Pseudo-second-order kinetic models of MK (b) and MK/CQD (d). Both kinetics models were derived from data of removal of 10 ppm of MB.

DOI: http://dx.doi.org/10.xxxxx/ijost.vXiX
p- ISSN 2528-1410 e- ISSN 2527-8045

Table 3. Adsorption kinetic model parameters of 10-ppm MB removal.

Sample	q_e (mg/g), exp.	Pseudo-first-order kinetic			Pseudo-second-order kinetic			
		q_e (mg/g), calc.	k_1 (min^{-1})	R^2	q_e (mg/g), calc.	k_2 (g/mg.min)	R^2	h (mg/g.min)
MK (5g)	119.748	68.573	0.0103	0.744	119.7605	0.000259	0.983	3.708
MK/CQD(10)	123.708	71.848	0.0154	0.887	127.551	0.000271	0.991	4.409
MK/CQD(20)	143.126	63.567	0.0169	0.789	145.138	0.000412	0.996	8.689
MK/CQD(40)	154.065	62.355	0.0155	0.69	155.521	0.000435	0.997	10.515

The pseudo-first-order and pseudo-second-order kinetics were employed as kinetic models, and corresponding equations for both models are expressed in Eqs. (3) and (4) (Zhang *et al*., 2019b):

$$\ln(q_e - q_t) = \ln q_e - k_1 t \quad (3)$$

$$t/q_t = \frac{1}{k_2 q_e^2} + \frac{t}{q_e} \quad (4)$$

where q_e and q_t are adsorption capacity at equilibrium and at a certain time interval (t) respectively. k_1 and k_2 are the rate constants for pseudo-first-order and pseudo-second-order kinetics, respectively. The fitting of experimental data for both kinetic models showed high linear regression for pseudo-second-order kinetics (R^2 = 0.99) (**Table 3**).

The calculated q_e values also exhibited high similarity with experimental q_e values. Therefore, the adsorption occurred with chemisorption as the rate-limiting step. Similar observations were reported by Pirhaji *et al*. (2020) and Niu *et al*. (2019), where halloysite/GO and coal-series kaolin were used to remove MB, and the adsorption displayed pseudo-second-order kinetics.

Among all samples, MK/CQD(40) provided the highest adsorption capacity at 154.065 mg/g and the highest rate constant at 4.35 × 10^{-4}. The initial sorption rate, h, could reach up to 10 mg/g.min for MK/CQD(40). The adsorption capacity value was quite remarkable for kaolin, and comparable to other kaolin samples, as presented in **Table 4**. Therefore, the composite material has the potential to be used as an adsorbent for dye removal, and even for the treatment of high dye concentrations.

Table 4. Comparison of kaolin samples' maximum adsorption.

Material	Maximum adsorption (mg/g)	Reference
Eucalyptus bark/kaolin clay	71.48	(Tan & Sen, 2020)
Kaolin/$CuFe_2O_4$	120.48	(Boushehrian *et al*., 2020)
Graphene oxide/kaolin	4.818	(Lertcumfu *et al*., 2020)
Aluminosilicates with kaolinite and halloysite structures	100	(Golubeva *et al*., 2020)
Tamazert kaolin modified with dimethyl sulfoxide	34.64	(Lellou *et al*., 2020)
Saudi red clay	50.25	(Khan, 2020)
Iraqi red kaolin	240.4	(Jawad & Abdulhameed, 2020)
Activated kaolinite by Fe_3O_4	171	(Asuha *et al*., 2020)
Kaolin nanospheres	184.9	(Zhang *et al*., 2019b)
Kaolin/CQD	154.065	This study

DOI: http://dx.doi.org/10.xxxxx/ijost.vXiX
p- ISSN 2528-1410 e- ISSN 2527-8045

4.3.2. Point of zero charges of MK and MK/CQD

The pHpzc was determined at specific pH when the net charge on the surface of the material was zero (Chung Hui *et al*., 2021; Patawat *et al*., 2020). As depicted in **Figure 11**, the pHpzc values for MK, MK/CQD(10), MK/CQD(20), and MK/CQD(40) were 4.25, 4.2, 4.78, and 4.3, respectively. Since the solution pH for MB removal was higher than pHpzc at neutral pH, the adsorbent surface was negatively charged due to deprotonation of the surface.

This improved the adsorption of positively charged MB on the adsorbent surface (Chung Hui *et al*., 2021; Li *et al*., 2018; Patawat *et al*., 2020). This shows that MK and MK/CQD are effective for the adsorption of MB. When the solution pH is lower than pHpzc, the excess H^+ is expected to inhibit the adsorption of MB (Li *et al*., 2018).

4.3.3. Effect of initial MB concentration

The comparison of performance between MK/CQD(40) and MK at different MB concentrations is presented in **Figure 12**. The material could remove approximately 96% of 5-ppm MB and 50% of 20-ppm MB. **Figure 12** also shows the difference in performance between MK and MK/CQD(40). MK/CQD(40) performed better than MK with more removal by 5, 17, 20, and 16%, for 5, 10, 15, and 20 ppm of MB, respectively. From these results, MK/CQD showed the potential to be applied for a wide range of dye concentrations with remarkable removal performance.

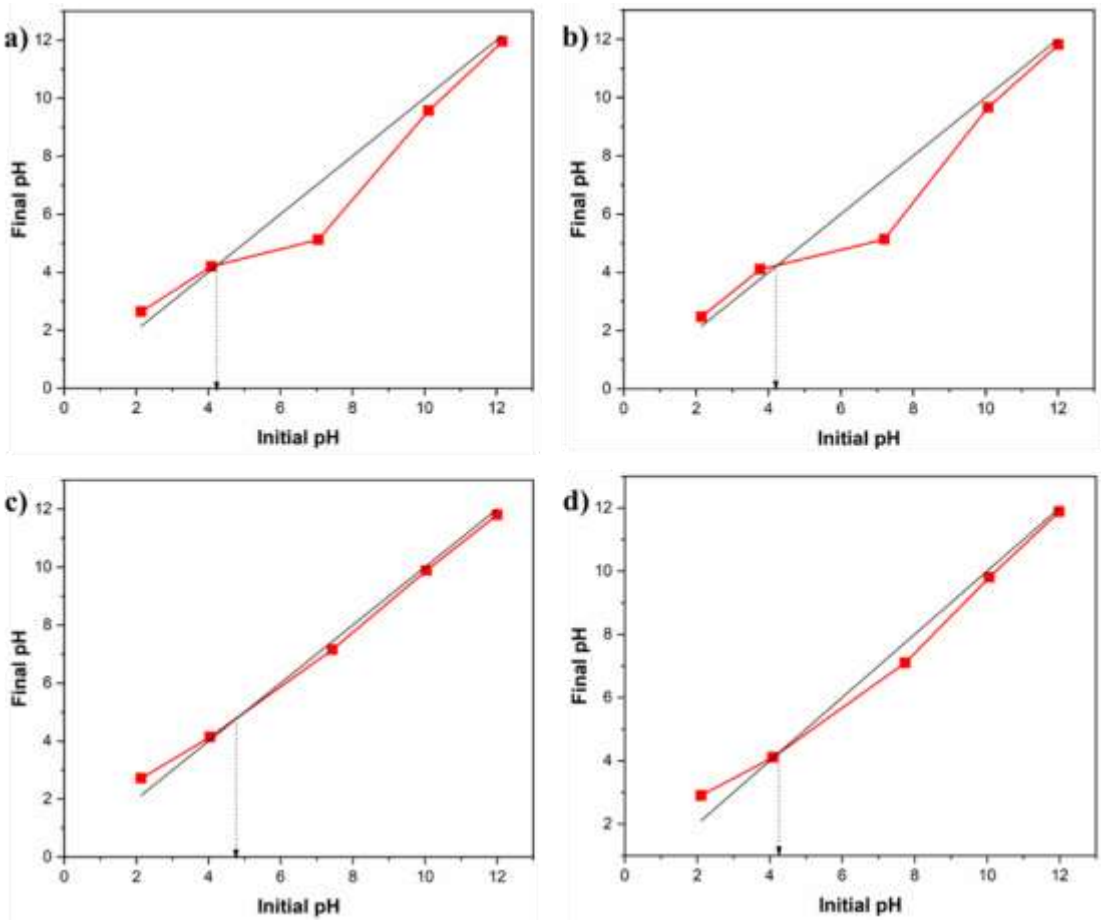

Figure 11. Determination of point zero charges for a) MK, b) MK/CQD(10), c) MK/CQD(20), and d) MK/CQD(40).

DOI: http://dx.doi.org/10.xxxxx/ijost.vXiX
p- ISSN 2528-1410 e- ISSN 2527-8045

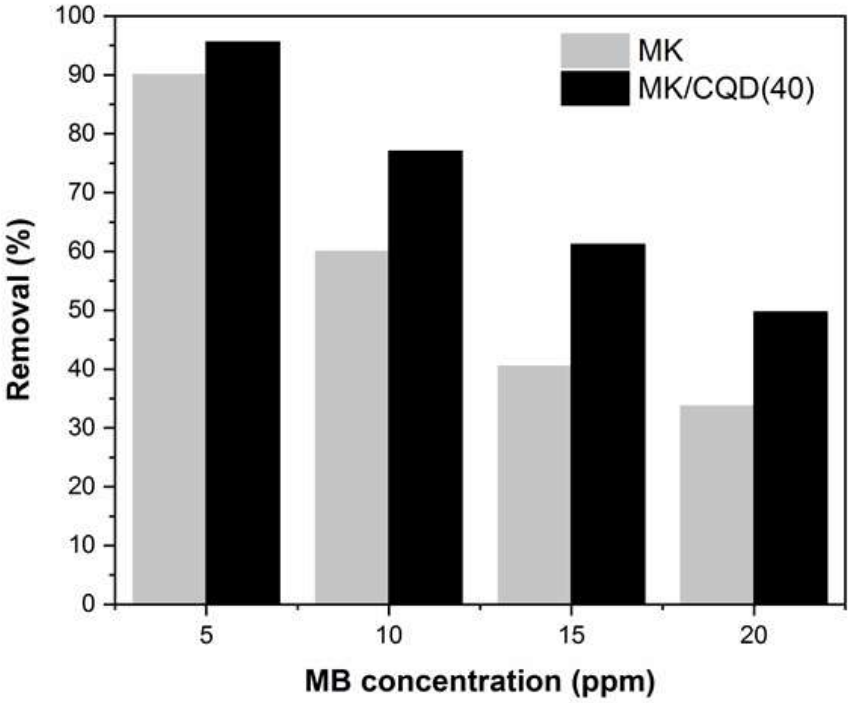

Figure 12. MB removal at various initial concentrations.

4.3.4. Recyclability of adsorbent

The recyclability of adsorbent was studied for MK/CQD(40) using 10-ppm MB. As shown in **Figure 13**, MB removal achieved 70.6% after cycles 1 and 2. Further reuse until cycle 4, reported decent MB removal at 64.3%.

The decreasing performance of MB removal could be due to the lodging of MB on the pores of MK/CQD(40), which cannot be removed from washing (Zhang *et al.*, 2019a). Despite that, the results show that the composite of MK/CQD has good regeneration ability, which can be used to treat high concentrations of dye.

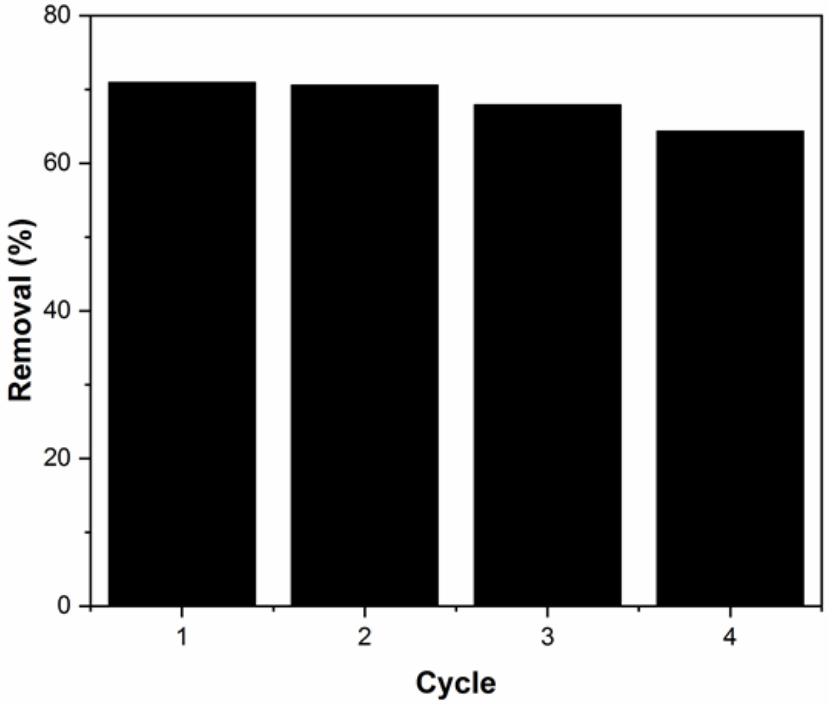

Figure 13. Recyclability of MK/CQD(40) for 10 ppm of MB.

DOI: http://dx.doi.org/10.xxxxx/ijost.vXiX
p- ISSN 2528-1410 e- ISSN 2527-8045

5. CONCLUSION

The modification of kaolin through heating at high temperature and acid-alkali treatment has changed its phase to MK and improved its surface area. However, further improvements can be achieved by incorporating CQDs into a kaolin matrix. The surface area can be improved up to 4 times, and the removal of MB increased by 2-folds. The incorporation of CQDs transformed the kaolin into a porous structure with more active sites. MK/CQD(40) exhibited good potential for reusability, where the composite retains more than 60% of MB removal after 4 cycles of usage.

6. ACKNOWLEDGMENT

We would like to acknowledge the research grant from YUTP International Collaborative Research Fund 015ME0-256, and the UiTM Special Research Grant with file no. RMC: 600-RMC/GPK 5/3 (118/2020).

7. AUTHORS' NOTE

The authors declare that there is no conflict of interest regarding the publication of this article. The authors confirmed that the paper is free of plagiarism.

8. REFERENCES

Alfred, M. O., Omorogie, M. O., Bodede, O., Moodley, R., Ogunlaja, A., Adeyemi, O. G., and Unuabonah, E. I. (2020). Solar-active clay-TiO2 nanocomposites prepared via biomass assisted synthesis: Efficient removal of ampicillin, sulfamethoxazole and artemether from water. *Chemical Engineering Journal*, *398*, 125544.

Anshar, A. M., Taba, P., and Raya, I. (2016). Kinetic and thermodynamics studies the adsorption of phenol on activated carbon from rice husk activated by ZnCl2. *Indonesian Journal of Science and Technology*, *1*(1), 47-60.

Asuha, S., Fei, F., Wurendaodi, W., Zhao, S., Wu, H., and Zhuang, X. (2020). Activation of kaolinite by a low-temperature chemical method and its effect on methylene blue adsorption. *Powder Technology*, *361*, 624-632.

Awad, A. M., Shaikh, S. M., Jalab, R., Gulied, M. H., Nasser, M. S., Benamor, A., and Adham, S. (2019). Adsorption of organic pollutants by natural and modified clays: a comprehensive review. *Separation and Purification Technology*, *228*, 115719.

Boukhemkhem, A., and Rida, K. (2017). Improvement adsorption capacity of methylene blue onto modified Tamazert kaolin. *Adsorption Science and Technology*, *35*(9-10), 753-773.

Boushehrian, M. M., Esmaeili, H., and Foroutan, R. (2020). Ultrasonic assisted synthesis of Kaolin/CuFe2O4 nanocomposite for removing cationic dyes from aqueous media. *Journal of Environmental Chemical Engineering*, *8*(4), 103869.

Caballero, L. R., Paiva, M. d. D. M., Fairbairn, E. d. M. R., and Toledo Filho, R. D. (2019). Thermal, mechanical and microstructural analysis of metakaolin based geopolymers. *Materials Research*, *22*, 1-8.

Chai, J. B., Au, P. I., Mubarak, N. M., Khalid, M., Ng, W. P. Q., Jagadish, P., and Abdullah, E. C. (2020). Adsorption of heavy metal from industrial wastewater onto low-cost Malaysian kaolin clay–based adsorbent. *Environmental Science and Pollution Research*, *27*(12), 13949-13962.

Chargui, H., Hajjaji, W., Wouters, J., Yans, J., and Jamoussi, F. (2018). Direct orange 34 dye fixation by modified kaolin. *Clay Minerals*, *53*(2), 271-287.

Chung Hui, K., Lun Ang, W., and Soraya Sambudi, N. (2021). Nitrogen and bismuth-doped rice husk-derived carbon quantum dots for dye degradation and heavy metal removal. *Journal of Photochemistry and Photobiology A: Chemistry*, *418*, 113411.

Chung, H. K., Wongso, V., Sambudi, N. S., and Isnaeni. (2020). Biowaste-derived carbon dots/hydroxyapatite nanocomposite as drug delivery vehicle for acetaminophen. *Journal of Sol-Gel Science and Technology*, *93*(1), 214-223.

Çiftçi, H. (2022). Removal of methylene blue from water by ultrasound-assisted adsorption using low-cost bentonites. *Chemical Physics Letters*, *802*, 139758.

David, M. K., Okoro, U. C., Akpomie, K. G., Okey, C., and Oluwasola, H. O. (2020). Thermal and hydrothermal alkaline modification of kaolin for the adsorptive removal of lead(II) ions from aqueous solution. *SN Applied Sciences*, *2*(6), 1134.

de la Luz-Asunción, M., Pérez-Ramírez, E. E., Martínez-Hernández, A. L., García-Casillas, P. E., Luna-Bárcenas, J. G., and Velasco-Santos, C. (2020). Adsorption and kinetic study of Reactive Red 2 dye onto graphene oxides and graphene quantum dots. *Diamond and Related Materials*, *109*, 108002.

de Oliveira, M. C. A., de L. Oliveira, E. G., Pires, I. C. B., Candido, I. C. M., Rakov, N., de Oliveira, H. P., and Maciel, G. S. (2020). Carbon dots-doped electrospun fibers for simultaneous metal ion detection and adsorption of dyes. *Advanced Fiber Materials*, *2*(6), 302-313.

Dewi, R., Shamsuddin, N., Bakar, M. S. A., Santos, J. H., Bilad, M. R., and Lim, L. H. (2021). Progress in emerging contaminants removal by adsorption/membrane filtration-based technologies: A review. *Indonesian Journal of Science and Technology*, *6*(3), 577-618.

Fadillah, G., Yudha, S. P., Sagadevan, S., Fatimah, I., and Muraza, O. (2020). Magnetic iron oxide/clay nanocomposites for adsorption and catalytic oxidation in water treatment applications. *Open Chemistry*, *18*(1), 1148-1166.

Fadzil, M. A., Nurhasri, M. M., Norliyati, M. A., Hamidah, M. S., Ibrahim, M. W., and Assrul, R. Z. (2017). Characterization of kaolin as nano material for high quality construction. *MATEC Web of Conferences*, *103*, 09019.

Fatimah, S., Ragadhita, R., Al Husaeni, D. F., and Nandiyanto, A. B. D. (2010). How to calculate crystallite size from x-ray diffraction (XRD) using Scherrer method. *ASEAN Journal of Science and Engineering*, *2*(1), 65-76.

Fei, F., Gao, Z., Wu, H., Wurendaodi, W., Zhao, S., and Asuha, S. (2020). Facile solid-state synthesis of Fe3O4/kaolinite nanocomposites for enhanced dye adsorption. *Journal of Solid State Chemistry*, *291*, 121655.

Ferrazzo, S. T., Tímbola, R. d. S., Bragagnolo, L., Prestes, E., Korf, E. P., Prietto, P. D. M., and Ulsen, C. (2020). Effects of acidic attack on chemical, mineralogical, and morphological properties of geomaterials. *Environmental Science and Pollution Research*, *27*(30), 37718-37732.

DOI: http://dx.doi.org/10.xxxxx/ijost.vXiX
p- ISSN 2528-1410 e- ISSN 2527-8045

Fiandini, M., Ragadhita, R. I. S. T. I., Nandiyanto, A. B. D., and Nugraha, W. C. (2020). Adsorption characteristics of submicron porous carbon particles prepared from rice husk. *Journal of Engineering Science and Technology*, *15*, 022-031.

Gasparini, E., Tarantino, S. C., Ghigna, P., Riccardi, M. P., Cedillo-González, E. I., Siligardi, C., and Zema, M. (2013). Thermal dehydroxylation of kaolinite under isothermal conditions. *Applied Clay Science*, *80*, 417-425.

Golubeva, O. Y., Alikina, Y. A., and Kalashnikova, T. A. (2020). Influence of hydrothermal synthesis conditions on the morphology and sorption properties of porous aluminosilicates with kaolinite and halloysite structures. *Applied Clay Science*, *199*, 105879.

Guggenheim, s., and Martin, R. T. (1995). Definition of clay and clay mineral: joint report of the AIPEA and CMS Nomenclature Committees. *Clay Minerals*, *30*(3), 257-259.

He, H., Chai, K., Wu, T., Qiu, Z., Wang, S., and Hong, J. (2022). Adsorption of rhodamine b from simulated waste water onto kaolin-bentonite composites. *Materials*, *15*(12), 4058.

He, K., Chen, G., Zeng, G., Chen, A., Huang, Z., Shi, J., and Hu, L. (2018). Enhanced removal performance for methylene blue by kaolin with graphene oxide modification. *Journal of the Taiwan Institute of Chemical Engineers*, *89*, 77-85.

Hens, S. C., Shenderova, O., and Turner, S. (2012). Producing photoluminescent species from sp2 carbons. *Fullerenes, Nanotubes and Carbon Nanostructures*, *20*(4-7), 502-509.

Jawad, A. H., and Abdulhameed, A. S. (2020). Mesoporous Iraqi red kaolin clay as an efficient adsorbent for methylene blue dye: Adsorption kinetic, isotherm and mechanism study. *Surfaces and Interfaces*, *18*, 100422.

Kandisa, R. V., Saibaba, K. N., Shaik, K. B., and Gopinath, R. (2016). Dye removal by adsorption: a review. *Journal of bioremediation and Biodegradation*, *7*(6), 371.

Katheresan, V., Kansedo, J., and Lau, S. Y. (2018). Efficiency of various recent wastewater dye removal methods: A review. *Journal of Environmental Chemical Engineering*, *6*(4), 4676-4697.

Khan, I., Ullah, H., Khairun Azizi, A., Sufian, S., Man, Z., Siyal, A., and Rehman, M. (2017). The pyrolysis kinetics of the conversion of Malaysian kaolin to metakaolin. *Applied Clay Science*, *146*, 152-161.

Khan, M. I. (2020). Adsorption of methylene blue onto natural Saudi Red Clay: isotherms, kinetics and thermodynamic studies. *Materials Research Express*, *7*(5), 055507.

Khuluk, R. H., and Rahmat, A. (2019). Removal of methylene blue by adsorption onto activated carbon from coconut shell (Cocous Nucifera L.). *Indonesian Journal of Science and Technology*, *4*(2), 229-240.

Kuila, U., and Prasad, M. (2013). Specific surface area and pore-size distribution in clays and shales. *Geophysical Prospecting*, *61*(2), 341-362.

DOI: http://dx.doi.org/10.xxxxx/ijost.vXiX
p- ISSN 2528-1410 e- ISSN 2527-8045

Lan, T., Li, P., Rehman, F. U., Li, X., Yang, W., and Guo, S. (2019). Efficient adsorption of Cd2+ from aqueous solution using metakaolin geopolymers. *Environmental Science and Pollution Research*, *26*(32), 33555-33567.

Lellou, S., Kadi, S., Guemou, L., Schott, J., and Benhebal, H. (2020). Study of methylene blue adsorption by modified kaolinite by dimethyl sulfoxide. *Ecological Chemistry and Engineering S-Chemia I Inzynieria Ekologiczna S*, *27*(2), 225-239.

Lertcumfu, N., Jaita, P., Thammarong, S., Lamkhao, S., Tandorn, S., Randorn, C., and Rujijanagul, G. (2020). Influence of graphene oxide additive on physical, microstructure, adsorption, and photocatalytic properties of calcined kaolinite-based geopolymer ceramic composites. *Colloids And Surfaces A: Physicochemical And Engineering Aspects*, *602*, 125080.

Li, F., Li, T., Sun, C., Xia, J., Jiao, Y., and Xu, H. (2017). Selenium-doped carbon quantum dots for free-radical scavenging. *Angewandte Chemie International Edition*, *56*(33), 9910-9914.

Li, X.-y., Han, D., Xie, J.-f., Wang, Z.-b., Gong, Z.-q., and Li, B. (2018). Hierarchical porous activated biochar derived from marine macroalgae wastes (Enteromorpha prolifera): facile synthesis and its application on Methylene Blue removal. *RSC Advances*, *8*(51), 29237-29247.

Liu, F., Zhang, W., Chen, W., Wang, J., Yang, Q., Zhu, W., and Wang, J. (2017a). One-pot synthesis of NiFe2O4 integrated with EDTA-derived carbon dots for enhanced removal of tetracycline. *Chemical Engineering Journal*, *310*, 187-196.

Liu, K., Luo, L., Zhou, W., Yang, J., Xiao, H., Hong, Z., and Yang, H. (2013). Study of behaviors of aluminum overlayers deposited on uranium via AES, EELS, and XPS. *Applied Surface Science*, *270*, 184–189.

Liu, X., Li, J. X., Huang, Y. S., Wang, X. X., Zhang, X. D., and Wang, X. K. (2017b). Adsorption, aggregation, and deposition behaviors of carbon dots on minerals. *Environmental Science and Technology*, *51*(11), 6156-6164.

Liu, X., Li, J. X., Wu, X. H., Zeng, Z., Wang, X. L., Hayat, T., and Zhang, X. D. (2017). Adsorption of carbon dots onto Al2O3 in aqueous: Experimental and theoretical studies. *Environmental Pollution*, *227*, 31-38.

Liu, X., Wu, Y., Li, M., Jiang, J., Guo, L., Wang, W., and Duan, P. (2020). Effects of graphene oxide on microstructure and mechanical properties of graphene oxide-geopolymer composites. *Construction and Building Materials*, *247*, 118544.

Long, C., Jiang, Z., Shangguan, J., Qing, T., Zhang, P., and Feng, B. (2021). Applications of carbon dots in environmental pollution control: A review. *Chemical Engineering Journal*, *406*, 126848.

Loutfi, M., Mariouch, R., Mariouch, I., Belfaquir, M., and ElYoubi, M. S. (2022). Adsorption of methylene blue dye from aqueous solutions onto natural clay: Equilibrium and kinetic studies. *Materials Today: Proceedings*, *2022*, 412.

Meigoli Boushehrian, M., Esmaeili, H., and Foroutan, R. (2020). Ultrasonic assisted synthesis of Kaolin/CuFe2O4 nanocomposite for removing cationic dyes from aqueous media. *Journal of Environmental Chemical Engineering*, *8*(4), 103869.

DOI: http://dx.doi.org/10.xxxxx/ijost.vXiX
p- ISSN 2528-1410 e- ISSN 2527-8045

Mohapi, M., Sefadi, J. S., Mochane, M. J., Magagula, S. I., and Lebelo, K. (2020). Effect of LDHs and other clays on polymer composite in adsorptive removal of contaminants: a review. *Crystals*, *10*(11), 957.

Mudgal, M., Singh, A., Chouhan, R. K., Acharya, A., and Srivastava, A. K. (2021). Fly ash red mud geopolymer with improved mechanical strength. *Cleaner Engineering and Technology*, *4*, 100215.

Mustapha, S., Ndamitso, M., Abdulkareem, A., Tijani Oladejo, J., Mohammed, A., and Shuaib, D. T. (2019). Potential of using kaolin as a natural adsorbent for the removal of pollutants from tannery wastewater. *Heliyon*, *5*, e02923.

Mustapha, S., Tijani, J. O., Ndamitso, M. M., Abdulkareem, S. A., Shuaib, D. T., Mohammed, A. K., and Sumaila, A. (2020). The role of kaolin and kaolin/ZnO nanoadsorbents in adsorption studies for tannery wastewater treatment. *Scientific Reports*, *10*(1), 13068.

Nandiyanto, A. B. D. A., Nissa Nur; Taufik, Refika Safitri Rizkia. (2022a). Investigation of adsorption performance of calcium carbonate microparticles prepared from eggshells waste. *Journal of Engineering Science and Technology*, *17*(3), 1934-1943.

Nandiyanto, A. B. D., Oktiani, R., and Ragadhita, R. (2019). How to read and interpret FTIR spectroscope of organic material. *Indonesian Journal of Science and Technology*, *4*(1), 97-118.

Nandiyanto, A. B. D., Putri, S. R., Anggraeni, S., Kurniwan, T. (2022b). Isotherm adsorption OF 3000-µm natural zeolite. *Journal of Engineering Science and Technology*, *17*(4), 2447-2460.

Natarajan, S., Bajaj, H. C., and Tayade, R. J. (2018). Recent advances based on the synergetic effect of adsorption for removal of dyes from waste water using photocatalytic process. *Journal of Environmental Sciences*, *65*, 201-222.

Niu, S., Xie, X., Wang, Z., Zheng, L., Gao, F., and Miao, Y. (2021). Enhanced removal performance for Congo red by coal-series kaolin with acid treatment. *Environmental Technology*, *42*(10), 1472-1481.

Nugraha, M. W., Zainal Abidin, N. H., Supandi, and Sambudi, N. S. (2021). Synthesis of tungsten oxide/ amino-functionalized sugarcane bagasse derived-carbon quantum dots (WO3/N-CQDs) composites for methylene blue removal. *Chemosphere*, *277*, 130300.

Obinna, E. M. (2022). Physicochemical properties of human hair using Fourier transform infra-red (FTIR) and scanning electron microscope (SEM). *ASEAN Journal for Science and Engineering in Materials*, *1*(2), 71-74.

Patawat, C., Silakate, K., Chuan-Udom, S., Supanchaiyamat, N., Hunt, A. J., and Ngernyen, Y. (2020). Preparation of activated carbon from Dipterocarpus alatus fruit and its application for methylene blue adsorption. *RSC Advances*, *10*(36), 21082-21091.

Pillay, D. L., Olalusi, O. B., Awoyera, P. O., Rondon, C., Echeverría, A. M., and Kolawole, J. T. (2020). A review of the engineering properties of metakaolin based concrete: Towards combatting chloride attack in coastal/marine structures. *Advances in Civil Engineering*, *2020*, 1-13.

DOI: http://dx.doi.org/10.xxxxx/ijost.vXiX
p- ISSN 2528-1410 e- ISSN 2527-8045

Prihastuti, H., and Kurniawan, T. (2022). Conversion of indonesian coal fly ash into zeolites for ammonium adsorption. *ASEAN Journal for Science and Engineering in Materials*, *1*(2), 75-84.

Ragadhita, R., and Nandiyanto, A. B. D. (2021). How to calculate adsorption isotherms of particles using two-parameter monolayer adsorption models and equations. *Indonesian Journal of Science and Technology*, *6*(1), 205-234.

Ragadhita, R., and Nandiyanto, A. B. D. (2022). Curcumin adsorption on zinc imidazole framework-8 particles: Isotherm adsorption using Langmuir, Freundlich, Temkin, and Dubinin-Radushkevich models. *Journal of Engineering Science and Technology*, *17*(2), 1078-1089.

Ragadhita, R., Nandiyanto, A. B. D., Nugraha, W. C., and Mudzakir, A. (2019). Adsorption isotherm of mesopore-free submicron silica particles from rice husk. *Journal of Engineering Science and Technology*, *14*(4), 2052-2062.

Raj, A. M., and Chirayil, G. T. (2017). Tunable direct band gap photoluminescent organic semiconducting nanoparticles from lignite. *Scientific Reports*, *7*(1), 1-9.

Rani, U. A., Ng, L. Y., Ng, C. Y., and Mahmoudi, E. (2020). A review of carbon quantum dots and their applications in wastewater treatment. *Advances in Colloid and Interface Science*, *278*, 102124.

Rashad, A. M. (2013). Metakaolin as cementitious material: History, scours, production and composition – A comprehensive overview. *Construction and Building Materials*, *41*, 303-318.

Ratlam, C., Phanichphant, S., and Sriwichai, S. (2020). Development of dopamine biosensor based on polyaniline/carbon quantum dots composite. *Journal of Polymer Research*, *27*(7), 1-12.

Sen Gupta, S., and Bhattacharyya, K. G. (2012). Adsorption of heavy metals on kaolinite and montmorillonite: A review. *Physical Chemistry Chemical Physics*, *14*(19), 6698-6723.

Shi, W., Guo, F., Wang, H., Liu, C., Fu, Y., Yuan, S., and Kang, Z. (2018). Carbon dots decorated magnetic ZnFe2O4 nanoparticles with enhanced adsorption capacity for the removal of dye from aqueous solution. *Applied Surface Science*, *433*, 790-797.

Shu, Z., Li, T. T., Zhou, J., Chen, Y., Yu, D. X., and Wang, Y. X. (2014). Template-free preparation of mesoporous silica and alumina from natural kaolinite and their application in methylene blue adsorption. *Applied Clay Science*, *102*, 33-40.

Sukamto, S., and Rahmat, A. (2023). Evaluation of ftir, macro and micronutrients of compost from black soldier fly residual: in context of its use as fertilizer. *ASEAN Journal of Science and Engineering*, *3*(1), 21-30.

Sullivan, M. S., Chorzepa, M. G., Hamid, H., Durham, S. A., and Kim, S. S. (2018). Sustainable materials for transportation infrastructures: Comparison of three commercially-available metakaolin products in binary cementitious systems. *Infrastructures*, *3*(3), 17.

Tan, T. C. N., and Sen, T. K. (2020). Aqueous-phase methylene blue (MB) dye removal by mixture of eucalyptus bark (EB) biomass and kaolin clay (KC) adsorbents: kinetics,

DOI: http://dx.doi.org/10.xxxxx/ijost.vXiX
p- ISSN 2528-1410 e- ISSN 2527-8045

thermodynamics, and isotherm modeling. *Separation Science and Technology*, *55*(6), 1036-1050.

Thommes, M., Kaneko, K., Neimark, A. V., Olivier, J. P., Rodriguez-Reinoso, F., Rouquerol, J., and Sing, K. S. W. (2015). Physisorption of gases, with special reference to the evaluation of surface area and pore size distribution (IUPAC Technical Report). *Pure and Applied Chemistry*, *87*(9-10), 1051-1069.

Vakalova, T. V., Reshetova, A. A., Revva, I. B., Rusinov, P. G., and Balamygin, D. I. (2019). Effect of thermochemical activation of clay raw materials on phase formation, microstructure and properties of aluminosilicate proppants. *Applied Clay Science*, *183*, 105335.

Valeev, D., Shoppert, A., Mikhailova, A., and Kondratiev, A. (2020). Acid and acid-alkali treatment methods of al-chloride solution obtained by the leaching of coal fly ash to produce sandy grade alumina. *Metals*, *10*(5), 585.

Wongso, V., Chen, C. J., Razzaq, A., Kamal, N. A., and Sambudi, N. S. (2019). Hybrid kaolin/TiO2 composite: Effect of urea addition towards an efficient photocatalyst for dye abatement under visible light irradiation. *Applied Clay Science*, *180*, 105158.

Wongso, V., Sambudi, N. S., and Sufian, S. (2021). The effect of hydrothermal conditions on photoluminescence properties of rice husk-derived silica-carbon quantum dots for methylene blue degradation. *Biomass Conversion and Biorefinery*, *11*(6), 2641-2654.

Wongso, V., Sambudi, N. S., Sufian, S., Isnaeni, and Abdullah, B. (2019). The effect of pH in the synthesis of carbon quantum dots from rice husk on their photoluminescence properties. *IOP Conference Series: Earth and Environmental Science*, *268*, 012087.

Yahaya Pudza, M., Zainal Abidin, Z., Abdul Rashid, S., Md Yasin, F., Noor, A. S. M., and Issa, M. A. (2020). Eco-friendly sustainable fluorescent carbon dots for the adsorption of heavy metal ions in aqueous environment. *Nanomaterials*, *10*(2), 315.

Yang, J., Hou, B., Wang, J., Tian, B., Bi, J., Wang, N., and Huang, X. (2019). Nanomaterials for the removal of heavy metals from wastewater. *Nanomaterials*, *9*(3), 424.

Ye, N., Chen, Y., Yang, J., Liang, S., Hu, Y., Hu, J., and Xiao, B. (2017). Transformations of Na, Al, Si and Fe species in red mud during synthesis of one-part geopolymers. *Cement and Concrete Research*, *101*, 123-130.

Yin, W.-M., Wang, Y., Hou, Y.-C., Sun, Y., Zhang, J.-G., Sun, H.-L., and Guo, Y.-R. (2020). Petaloid-array hierarchically structured carbon Dots/Mg(OH)2 composite: Design, characterization and removal/recovery of cadmium via slowly releasing. *Chemical Engineering Journal*, *401*, 125961.

Yolanda, Y. D., and Nandiyanto, A. B. D. (2022). How to read and calculate diameter size from electron microscopy images. *ASEAN Journal of Science and Engineering Education*, *2*(1), 11-36.

Zainal Abidin, N. H., Wongso, V., Hui, K. C., Cho, K., Sambudi, N. S., Ang, W. L., and Saad, B. (2020). The effect of functionalization on rice-husks derived carbon quantum dots properties and cadmium removal. *Journal of Water Process Engineering*, *38*, 101634.

DOI: http://dx.doi.org/10.xxxxx/ijost.vXiX
p- ISSN 2528-1410 e- ISSN 2527-8045

Zare Pirhaji, J., Moeinpour, F., Mirhoseini Dehabadi, A., and Yasini Ardakani, S. A. (2020). Synthesis and characterization of halloysite/graphene quantum dots magnetic nanocomposite as a new adsorbent for Pb(II) removal from water. *Journal of Molecular Liquids*, *300*, 112345.

Zhang, Q., Zhang, Y., Chen, J., and Liu, Q. (2019). Hierarchical structure kaolinite nanospheres with remarkably enhanced adsorption properties for methylene blue. *Nanoscale Research Letters*, *14*(1), 1-9.

Zhang, T., Wang, W., Zhao, Y., Bai, H., Wen, T., Kang, S., and Komarneni, S. (2021). Removal of heavy metals and dyes by clay-based adsorbents: From natural clays to 1D and 2D nano-composites. *Chemical Engineering Journal*, *420*, 127574.

Zhang, Y., Chen, S., Feng, X., Yu, J., and Jiang, X. (2019b). Self-assembly of sponge-like kaolin/chitosan/reduced graphene oxide composite hydrogels for adsorption of Cr(VI) and AYR. *Environmental Science and Pollution Research*, *26*(28), 28898-28908.

DOI: http://dx.doi.org/10.xxxxx/ijost.vXiX
p- ISSN 2528-1410 e- ISSN 2527-8045